JOURNAL OF SANDWICH STRUCTURES & MATERIALS

Standard Article

Journal of Sandwich Structures and Materials
0(00) 1–27

DOI: 10.1177/1099636215603027
jsm.sagepub.com
SAGE

An accurate discrete model for web-core sandwich plates

Anup Pydah and K Bhaskar

Abstract

An accurate discrete model is presented here for the analysis of simply supported web-core sandwich plates. In this model, the face plates are analysed using the equations of 3D elasticity and for the webs a plane stress idealization is used to model the kinematics of transverse bending while simple one-dimensional classical models are employed for lateral bending and torsion. Thus, this model accounts for the non-classical effects of transverse shear deformation and transverse thickness-stretch in the face-plates and the webs. It is shown that this model is capable of accurately capturing the effects of secondary local bending of the face-plates between the webs on the displacement and stress fields. Results obtained by this rigorous approach are used to highlight the errors of the commonly used model based on the classical hairbrush hypothesis for the face-plates.

Keywords

Web-core sandwich plates, shear deformation, elasticity solution

Introduction

Sandwich plates are extremely efficient modular structures which possess high stiffness-to-weight ratios and the capability to be tailored according to design requirements. These attributes make them a popular structural choice in the aerospace, naval, automobile and other high-performance industries.

Sandwich plates consist of two isotropic or orthotropic face-plates separated by a core which may be continuous – in the form of a metallic or a low-strength foam – or discrete – in the form of a hollow core consisting of a corrugated

Aerospace Engineering Department, Indian Institute of Technology Madras, Chennai, India

Corresponding author:
K Bhaskar, Aerospace Engineering Department, Indian Institute of Technology Madras, Chennai 600036, India.
Email: kbhas@ae.iitm.ac.in

sheet or a number of discrete webs running in one direction parallel to the face-plates, or square or hexagonal cell honeycombs, or other similar configurations [1].

Foam-core sandwich plates are usually analysed using a discrete three-layer approach wherein the core and face-plates are modelled separately, along with suitable stress and displacement continuity conditions at the interfaces. The typical approximations made in such an approach are that the face-plates follow classical plate – or even membrane – kinematics, while the core resists only shear [2]. However, the increasing use of composite face-plates, which have transverse shear stiffness much smaller than bending stiffness as compared to metallic plates, has led to the advent of models based on the first-order shear deformation theory (FSDT) [3] as well as the three-dimensional elasticity theory for face-plates, also besides the core [4,5].

For web-core, honeycomb core or other such discrete core plates, considerable emphasis has been laid on developing ''continuum-based'' models wherein the discrete core is replaced by an equivalent homogeneous orthotropic layer [6]; this is obviously easier than discrete modelling of the core structural configuration. The validity of such homogenization is established by comparing it with various finite element models [7,8]. While this approach does simplify the analysis to a great extent, a major drawback is that the complex expressions developed for the stiffness parameters of a specific discrete core plate cannot be used for other core configurations [9]; hence significant work has been done on developing homogenization schemes for various discrete core configurations [10–12]. However, in any of these homogenized models, the structure loses its discrete nature, making it impossible to capture local effects like the secondary bending of the face-plates between the webs of a web-core sandwich plate. Burton et al. [13,14] conducted extensive numerical studies and concluded that global response quantities like strain energy components, vibrational frequencies etc. can be predicted accurately by the homogenized approach, but detailed local response components like stresses would require a higher-order discrete layer approach. They also concluded that the mechanical response of such structures is extremely sensitive to small variations in the effective material properties. For web-core sandwich plates, Romanoff et al. [15] developed a model which used a combination of the homogenized formulation based on the Reissner–Mindlin theory and a Kirchhoff plate analysis which captures the local bending of the face-plates to accurately predict stresses.

There have been a few attempts to discretely model the hollow structural core of certain sandwich plates [16,17]. These models treat the web core sheets as one-dimensional incompressible beams and capture their shear deformation using a FSDT while ignoring the shear deformations of the face-plates. Further, the out-of-plane effects of the webs including torsion and lateral bending are omitted.

In the above context, the objective of the present paper is to extend the kinematics of a discrete model, proposed recently by the authors for blade-stiffened plates [18,19], to web-core sandwich plates. In these references it was shown that

non-classical effects like transverse shear deformation and thickness-stretch play an important role in the kinematics of stiffened plates and that the errors of the classical theories are much more significant in stiffened plates than for corresponding unstiffened plates. It was also shown that the shear deformation of the plate is more significant than that of the stiffeners and must be captured unless the plate is extremely thin.

In the present extension of the above model to the discrete analysis of web-core sandwich plates, the face-plates are modelled using the full three-dimensional equations of elasticity while the webs are analysed using a plane-stress formulation for transverse bending, and Euler–Bernoulli hypothesis and Saint-Venant's theory of torsion, respectively, for lateral bending and twisting. Thus this model completely captures the non-classical effects of transverse shear deformation and thickness-stretch for the face-plates and the webs while completely neglecting such effects on lateral bending of the webs. This approach is first validated by comparing it with a full-3D finite element model of the face-plates as well as the webs. Later, results are generated for isotropic and orthotropic web-core plates of different thicknesses and configurations and are compared with models based on the classical Kirchhoff hypothesis for the face-plates to ascertain the importance of capturing these non-classical effects for the face-plates. Transverse deflections and stress results are tabulated for future comparisons.

Formulation

Consider a rectangular web-core sandwich plate of sides a, b (Figure 1) with simply supported edges of the shear-diaphragm type. The sandwich plate consists of two face-plates of thickness h_f separated by a set of n_w equally spaced unidirectional webs, each of height H and breadth B. The webs are integrally attached to the face-plates and are also taken to be simply supported at the ends of their length. In the present discrete formulation, the plate and the webs are modelled separately while maintaining suitable compatibility at the interfaces; this is explained in full detail below.

As the sandwich plate bends in the transverse z-direction, each web bends in the transverse (x–z) as well as the lateral (x–y) planes, and also twists along its length. The bending of the face-plates can be accurately analysed using the 3D equations of elasticity so as to completely capture the non-classical effects of transverse shear deformation and thickness-stretch. Transverse bending of the webs is analysed using a 2D plane stress formulation which completely accounts for vertical shear deformation (τ_{xz}) and normal strain (ε_z) effects. The other two modes of deformation of the web, namely torsion and lateral bending, are expected to be of lesser significance to the overall kinematics of the sandwich plate and are hence modelled using the one-dimensional classical Saint-Venant's free-warping torsion theory and the Euler-Bernoulli theory, respectively.

Consistent with the above formulations, a set of appropriate interface tractions are introduced, as explained below.

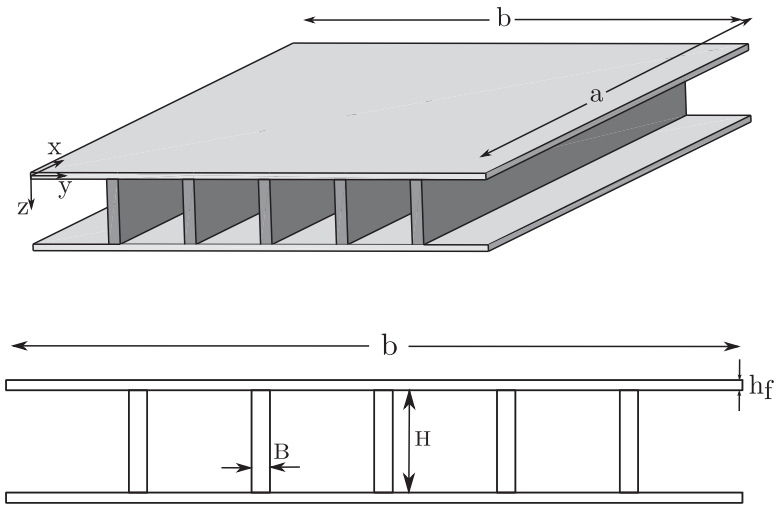

Figure 1. Web-core sandwich plate.

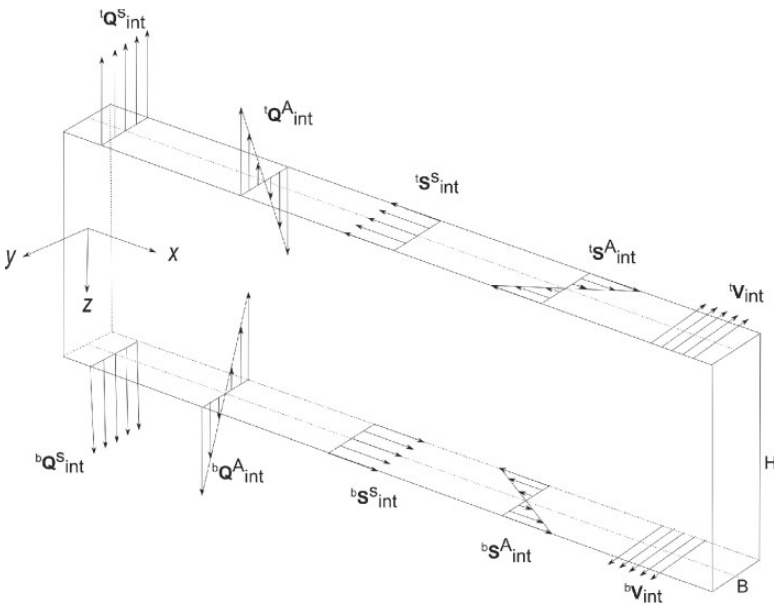

Figure 2. Interface tractions on a web.

The interface tractions

All three interface tractions are considered at the top and bottom of each web (Figure 2) with the possibility of a general variation across the interface

width B; these quantities correspond to the stresses σ_z, τ_{zx} and τ_{zy} on the interface plane x–y, and their directions, when positive as per the sign convention adopted here, are shown in the figure. Constant as well as linear antisymmetric variations along the breadth B of the interface patch are assumed for the transverse normal and in-plane shear tractions, while the out-of-plane shear traction is assumed to be constant along the breadth. The mathematical expressions for these tractions (for the i th web), as well as suitable series expansions for later use, are given below:

1. The transverse normal traction ${}^{p}Q_{\text{int}}(x, y)$ is taken as

$$ {}^{p}_{i}Q_{\text{int}} = {}^{p}_{i}Q^{S}_{\text{int}} + {}^{p}_{i}Q^{A}_{\text{int}} = \sum_{m=1}^{\infty} \left({}^{p}_{i}Q^{S}_{m} + {}^{p}_{i}Q^{A}_{m}.y\right) \sin\left(\frac{m\pi}{a}x\right) \tag{1} $$

2. The in-plane shear traction ${}^{p}S_{\text{int}}(x, y)$ is taken as

$$ {}^{p}_{i}S_{\text{int}} = {}^{p}_{i}S^{S}_{\text{int}} + {}^{p}_{i}S^{A}_{\text{int}} = \sum_{m=1}^{\infty} \left({}^{p}_{i}S^{S}_{m} + {}^{p}_{i}S^{A}_{m}.y\right) \cos\left(\frac{m\pi}{a}x\right) \tag{2} $$

3. The out-of plane shear traction ${}^{p}V_{\text{int}}(x, y)$ is taken as

$$ {}^{p}_{i}V_{\text{int}} = \sum_{m=1}^{\infty} {}^{p}_{i}V^{S}_{m} \sin\left(\frac{m\pi}{a}x\right) \tag{3} $$

where the superscripts S and A denote the symmetric and antisymmetric part of the tractions respectively, and the superscript p takes the values of t and b to denote the top or bottom of the web, respectively.

Analysis of the web

The plane stress idealization for the web captures the effects of the constant parts of the normal and in-plane shear tractions, ${}^{p}_{i}Q^{S}_{\text{int}}$ and ${}^{p}_{i}S^{S}_{\text{int}}$, while the classical Euler–Bernoulli beam theory and Saint-Venant's torsion formulation are used to analyse the lateral bending and torsion of the web due to the remaining traction components. The latter one-dimensional formulations require the tractions to be shifted to the centre line of the web and rewritten as loads and moments per unit length. The anti-symmetric parts of the normal tractions ${}^{p}_{i}Q^{A}_{\text{int}}$ are statically equivalent to torques per unit length ${}^{p}_{i}T_1(x)$, with the superscript p just to show the source of such torques. Shifting the out-of-plane shear tractions ${}^{p}_{i}V_{\text{int}}$ to the mid line results in a statically equivalent loading system consisting of lateral loads per unit length ${}^{p}_{i}q_l(x)$ and torques per unit length ${}^{p}_{i}T_2(x)$; once again, the superscript p indicates the source. The effect of the antisymmetric part of the in-plane shear tractions ${}^{p}_{i}S^{A}_{\text{int}}$

is to produce distributed moments per unit length ${}^{p}_{i}m_l(x)$. These are summarized below:

$$ {}^{p}_{i}T_1(x) = \int_{-\frac{B}{2}}^{\frac{B}{2}} {}^{p}_{i}Q^{A}_{\text{int}}.y\,\mathrm{d}y \;=\; \frac{B^3}{12}.\sum_{m=1}^{\infty} {}^{p}_{i}Q^{A}_{m}\sin\left(\frac{m\pi}{a}x\right) \tag{4} $$

$$ {}^{p}_{i}T_2(x) = {}^{p}_{i}V_{\text{int}}(x).B.\frac{H}{2} \;=\; \frac{BH}{2}.\sum_{m=1}^{\infty} {}^{p}_{i}V^{S}_{m}\sin\left(\frac{m\pi}{a}x\right) \tag{5} $$

$$ {}^{p}_{i}q_l(x) = {}^{p}_{i}V_{\text{int}}(x).B \;=\; B.\sum_{m=1}^{\infty} {}^{p}_{i}V^{S}_{m}\sin\left(\frac{m\pi}{a}x\right) \tag{6} $$

$$ {}^{p}_{i}m_l(x) = \int_{-\frac{B}{2}}^{\frac{B}{2}} {}^{p}_{i}S^{A}_{\text{int}}.y\,\mathrm{d}y \;=\; \frac{B^3}{12}.\sum_{m=1}^{\infty} {}^{p}_{i}S^{A}_{m}\cos\left(\frac{m\pi}{a}x\right) \tag{7} $$

with $p = t$ or b.

Transverse bending of the web. This analysis, due to the normal and shear tractions ${}^{p}_{i}Q^{S}_{\text{int}}$ and ${}^{p}_{i}S^{S}_{\text{int}}$, is carried out as a plane-stress problem in the x–z plane (Figure 2). Assuming that the web is specially orthotropic with the plane stress constitutive law

$$ \begin{Bmatrix} \sigma_x \\ \sigma_z \\ \tau_{xz} \end{Bmatrix} = \begin{bmatrix} Q_{11} & Q_{12} & 0 \\ Q_{12} & Q_{22} & 0 \\ 0 & 0 & Q_{55} \end{bmatrix} \begin{Bmatrix} \epsilon_x \\ \epsilon_z \\ \gamma_{xz} \end{Bmatrix} $$

the 2D equations of equilibrium can be written in terms of the displacements u and w along the x and z directions respectively, as

$$ \begin{aligned} Q_{11}u_{,xx} + Q_{55}u_{,zz} + (Q_{12} + Q_{55})w_{,xz} = 0 \\ (Q_{12} + Q_{55})u_{,xz} + Q_{55}w_{,xx,} + Q_{22}w_{,zz} = 0 \end{aligned} \tag{8} $$

Selection of displacement functions

$$ u(x,z) = \sum_{m=1}^{\infty} U(z)\cos\left(\frac{m\pi}{a}x\right) $$

$$ w(x,z) = \sum_{m=1}^{\infty} W(z)\sin\left(\frac{m\pi}{a}x\right) $$

ensure that the shear-diaphragm type simple support conditions

$$\text{at } x = 0,\ a; \quad w = 0, \quad \sigma_x = 0$$

for all z are satisfied a priori.

Substitution of the above displacement functions into (8) reduces them to a 4th order system of linear ordinary differential equations in z. Following the standard procedure of seeking solutions for $U(z)$ and $W(z)$ as

$$\left\{ \begin{array}{c} U \\ W \end{array} \right\} = \left\{ \begin{array}{c} U_0 \\ W_0 \end{array} \right\} \mathrm{e}^{sz}$$

one gets the auxiliary equation as

$$A' s^4 + B' s^2 + C' = 0 \tag{9}$$

where A', B', C' and D' are functions of the harmonic m and the material properties Q_{ij} of the web.

The nature of the roots of this equation dictates the final solution. For example, in the case of real and distinct roots, the final solution is of the form

$$u = \sum_{m=1}^{\infty} \left(\sum_{i=1}^{4} C_{1i} e^{s_i z} \right) \cos\left(\frac{m\pi}{a} x \right)$$

$$w = \sum_{m=1}^{\infty} \left(\sum_{i=1}^{4} C_{2i} e^{s_i z} \right) \sin\left(\frac{m\pi}{a} x \right) \tag{10}$$

Of the eight constants C_{1i}, C_{2i} (for each harmonic m), only four are independent. The inter-relationships are established by substituting the above displacement field into the ordinary differential equations and equating the coefficients of $\mathrm{e}^{s_i z}$ ($i = 1$ to 4) in each equation to 0.

The four independent constants for each m can be determined by enforcing the conditions:

a. at the top surface $z = -\frac{H}{2}$,

$$\sigma_z(x) = {}_i^t Q_{\text{int}}^S \quad \text{and} \quad \tau_{xz}(x) = {}_i^t S_{\text{int}}^S$$

b. at the bottom surface $z = \frac{H}{2}$,

$$\sigma_z(x) = {}_i^b Q_{\text{int}}^S \quad \text{and} \quad \tau_{xz}(x) = {}_i^b S_{\text{int}}^S$$

and are thus obtained in terms of ${}_i^p Q_m^S$ and ${}_i^p S_m^S$ (see equations (1) and (2)).

Lateral bending of the web. The analysis of the lateral bending of the web, due to lateral loads ${}_i^p q_l(x)$ per unit length and distributed moments ${}_i^p m_l(x)$ per unit length, is carried out using the classical beam theory.

The effect of these loads can be captured by starting with a displacement field as

$$v_b(x, y) = v_b(x)$$

$$u_b(x, y) = -y.v_{b,\,x}$$

The corresponding equations of equilibrium are

$$V_{l,\,x} = {}_i^t q_l - {}_i^b q_l \tag{11}$$

$$M_{l,\,x} + ({}_i^t m_l - {}_i^b m_l) + V_l = 0 \tag{12}$$

where V_l and M_l are the shear force and bending moment respectively, at any section of the beam.

Eliminating V_l from (11) and (12) yields

$$M_{l,\,xx} + ({}_i^t m_l - {}_i^b m_l)_{,\,x} + {}_i^t q_l - {}_i^b q_l = 0 \tag{13}$$

Using $\sigma_x = E_x \varepsilon_x = -E_x.y\ v_{b,xx}$ and obtaining the moment-curvature relations by appropriate integrations over the cross-sectional area A, the governing equation can be derived from (13) as

$$E_x.I_{zz} v_{b,\,xxxx} + ({}_i^t m_l - {}_i^b m_l)_{,\,x} + {}_i^t q_l - {}_i^b q_l = 0 \tag{14}$$

where I_{zz} is the area moment of inertia of the cross-section about the neutral axis passing through the centroid.

For simply supported boundary conditions at the ends given by

$$\text{at} \quad x = 0,\ a; \qquad v_b = M_l = 0$$

$$\text{i.e. } v_b = v_{b,\,xx} = 0,$$

a solution can be sought as

$$v_b(x) = \sum_{m=1}^{\infty} v_{bm} \sin\left(\frac{m\pi}{a} x\right)$$

Substitution of this in equation (14) yields v_{bm} in terms of ${}_i^p V_m^S$ and ${}_i^p S_m^A$ (see equations (6) and (7)).

Torsion of the web. The torsional analysis of the web is carried out using Saint-Venant's assumption that cross-sections of the web rotate as rigid bodies and warp freely. It needs to be noted that the web is subject to variable torques along its length, so this is a case of non-uniform torsion; however, since the warping constant is quite small for the open section webs considered here, it is neglected and the torque-twist relationship is simply taken as

$$T_x \approxeq G_{xz}.J.\theta,_x \tag{15}$$

where T_x is the the torque stress resultant, $\theta(x)$ is the rotation of a cross-section about its centre of twist and J is the torsional constant of the rectangular cross section given by [20]

$$J = H.B^3\left(\frac{1}{3} - \frac{64}{\pi^5}\frac{B}{H}\sum_{r=1,3,5..}^{\infty}\frac{1}{r^5}\tanh\left(\frac{r\pi H}{2B}\right)\right)$$

With respect to the torsional loads given by (4) and (5), the equation of motion for this system is

$$T_{x,x} =_i^t T_1 +_i^t T_2 -_i^b T_1 +_i^b T_2$$

Using (15), the governing equation can be derived as

$$G_{xz}.J.\theta,_{xx} =_i^t T_1 +_i^t T_2 -_i^b T_1 +_i^b T_2 \tag{16}$$

Corresponding to the shear-diaphragm boundary conditions

$$\text{at } x = 0,\ a: \qquad \theta = 0$$

a solution can be sought in the form

$$\theta(x) = \sum_{m=1}^{\infty}\theta_m\ \sin\left(\frac{m\pi x}{a}\right)$$

Substitution of this in equation (16) yields θ_m in terms of ${}_i^p Q_m^A$ and ${}_i^p V_m^S$ (see equations (4) and (5)).

The displacement components along the y and z directions due to twisting are given by

$$v_t(x, y, z) = -z.\theta(x)$$

$$w_t(x, y, z) = y.\theta(x)$$

The shear strain γ_{xy} (required later for enforcing compatibility between the face-plates and the webs) is found out using

$$\gamma_{xy} = \phi,_z/G_{xy} \tag{17}$$

where ϕ is the Prandtl stress function given by [20]

$$\phi(x, y, z) = \frac{8G_{xy}B^2\theta,_x}{\pi^3}.\sum_{r=1,3,5..}^{\infty}\frac{1}{r^3}.\left(1-\frac{\cosh(r\pi z/B)}{\cosh(r\pi H/2B)}\right).\sin(r\pi/2).\cos\left(\frac{r\pi y}{B}\right)$$

This concludes the analysis of the web. By virtue of the principle of superposition, the total displacement field is simply a sum of the displacement contributions from each of the three-deformation modes of the web. While the web also undergoes warping displacement u due to torsion, this displacement is not of any interest in this analysis. This is because the displacement continuity between the plate and webs will be enforced (see section Analysis of the overall structure) only along the centre line of the interface patch, and along this line the warping displacement u is zero.

3D elasticity formulation for the face-plates

The simply supported face-plate of dimensions a x b x h_f is taken to be orthotropic with respect to the x–y–z axes and governed by the following constitutive law:

$$\begin{Bmatrix}\sigma_x\\ \sigma_y\\ \sigma_z\\ \tau_{yz}\\ \tau_{xz}\\ \tau_{xy}\end{Bmatrix} = \begin{bmatrix}C_{11} & C_{12} & C_{13} & 0 & 0 & 0\\ C_{12} & C_{22} & C_{23} & 0 & 0 & 0\\ C_{13} & C_{23} & C_{33} & 0 & 0 & 0\\ 0 & 0 & 0 & C_{44} & 0 & 0\\ 0 & 0 & 0 & 0 & C_{55} & 0\\ 0 & 0 & 0 & 0 & 0 & C_{66}\end{bmatrix}\begin{Bmatrix}\epsilon_x\\ \epsilon_x\\ \epsilon_x\\ \gamma_{yz}\\ \gamma_{xz}\\ \gamma_{xy}\end{Bmatrix}$$

For each face-plate the origin of the z coordinate is taken at its mid-plane. The 3D equations of equilibrium in terms of the displacements u, v and w along the x, y and z directions respectively are

$$C_{11}u,_{xx} + C_{66}u,_{yy} + C_{55}u,_{zz} + (C_{12} + C_{66})v,_{xy} + (C_{13} + C_{55})w,_{xz} = 0$$

$$\begin{aligned} C_{66}v_{,xx} + C_{22}v_{,yy} + C_{44}v_{,zz} + (C_{12} + C_{66})u_{,xy} + (C_{23} + C_{44})w_{,yz} = 0 \\ C_{55}w_{,xx} + C_{44}w_{,yy} + C_{33}w_{,zz} + (C_{13} + C_{55})u_{,xz} + (C_{23} + C_{44})v_{,yz} = 0 \end{aligned} \tag{18}$$

The displacement functions

$$u(x,y,z) = \sum_{m=1}^{\infty}\sum_{n=1}^{\infty} U(z)\cos\left(\frac{m\pi}{a}x\right)\sin\left(\frac{n\pi}{b}y\right)$$

$$v(x,y,z) = \sum_{m=1}^{\infty}\sum_{n=1}^{\infty} V(z)\sin\left(\frac{m\pi}{a}x\right)\cos\left(\frac{n\pi}{b}y\right)$$

$$w(x,y,z) = \sum_{m=1}^{\infty}\sum_{n=1}^{\infty} W(z)\sin\left(\frac{m\pi}{a}x\right)\sin\left(\frac{n\pi}{b}y\right)$$

satisfy the shear-diaphragm conditions of both face-plates

$$\text{at } x = 0,\ a; \quad w = 0, \quad v = 0, \quad \sigma_x = 0$$

$$\text{at } y = 0,\ b; \quad w = 0, \quad u = 0, \quad \sigma_y = 0$$

a priori, and reduce the problem to a 6th order system of linear ordinary differential equations.

Proceeding as done for the web by starting with

$$\begin{Bmatrix} U \\ V \\ W \end{Bmatrix} = \begin{Bmatrix} U_0 \\ V_0 \\ W_0 \end{Bmatrix} e^{sz}$$

one gets the auxiliary equation as

$$A\,s^6 + B\,s^4 + C\,s^2 + D = 0 \tag{19}$$

where A, B, C and D are functions of m, n and the material properties C_{ij}.

The nature of the roots of this auxiliary equation dictates the form of the final solution. For the case of real and distinct roots, the final solution is given by:

$$u = \sum_{m=1}^{\infty}\sum_{n=1}^{\infty}\left(\sum_{i=1}^{6} K_{1i}e^{s_i z}\right)\cos\left(\frac{m\pi}{a}x\right)\sin\left(\frac{n\pi}{b}y\right)$$

$$v = \sum_{m=1}^{\infty}\sum_{n=1}^{\infty}\left(\sum_{i=1}^{6} K_{2i}e^{s_i z}\right)\sin\left(\frac{m\pi}{a}x\right)\cos\left(\frac{n\pi}{b}y\right)$$
$$w = \sum_{m=1}^{\infty}\sum_{n=1}^{\infty}\left(\sum_{i=1}^{6} K_{3i}e^{s_i z}\right)\sin\left(\frac{m\pi}{a}x\right)\sin\left(\frac{n\pi}{b}y\right) \tag{20}$$

wherein only six constants (for each harmonic set $\{m, n\}$) are independent.

For the purpose of enforcing lateral surface conditions, the interface tractions ${}^{p}_{i}Q_{\text{int}}$, ${}^{p}_{i}S_{\text{int}}$ and ${}^{p}_{i}V_{\text{int}}$ acting over any i^{th} strip $0 \le x \le a$ and $(b^* - \frac{B}{2}) \le y \le (b^* + \frac{B}{2})$ need to be expressed in double series as

$${}^{p}_{i}Q_{\text{int}} = \sum_{m=1}^{\infty}\sum_{n=1}^{\infty}\left({}^{p}_{i}Q_{mn}\sin\left(\frac{m\pi}{a}x\right)\sin\left(\frac{n\pi}{b}y\right)\right) \tag{21}$$

$${}^{p}_{i}S_{\text{int}} = \sum_{m=1}^{\infty}\sum_{n=1}^{\infty}\left({}^{p}_{i}S_{mn}\cos\left(\frac{m\pi}{a}x\right)\sin\left(\frac{n\pi}{b}y\right)\right) \tag{22}$$

and

$${}^{p}_{i}V_{\text{int}} = \sum_{m=1}^{\infty}\sum_{n=1}^{\infty}\left({}^{p}_{i}V_{mn}\sin\left(\frac{m\pi}{a}x\right)\cos\left(\frac{n\pi}{b}y\right)\right) \tag{23}$$

where

$${}^{p}_{i}Q_{mn} = \frac{2}{b}\int_{(b^*-\frac{B}{2})}^{(b^*+\frac{B}{2})}({}^{p}_{i}Q^{S}_{m} + {}^{p}_{i}Q^{A}_{m}.(y - b^*))\sin\left(\frac{n\pi}{b}y\right)\mathrm{d}y$$

$${}^{p}_{i}S_{mn} = \frac{2}{b}\int_{(b^*-\frac{B}{2})}^{(b^*+\frac{B}{2})}({}^{p}_{i}S^{S}_{m} + {}^{p}_{i}S^{A}_{m}.(y - b^*))\sin\left(\frac{n\pi}{b}y\right)\mathrm{d}y$$

$${}^{p}_{i}V_{mn} = \frac{2}{b}\int_{(b^*-\frac{B}{2})}^{(b^*+\frac{B}{2})}{}^{p}_{i}V^{S}_{m}\sin\left(\frac{n\pi}{b}y\right)\mathrm{d}y$$

and $b^* = i^*b/(n_w + 1)$

The lateral boundary conditions for the top face-plate are:

a. at the top surface ($z = -\frac{h_f}{2}$),

$$\sigma_z(x, y) = -{}^{t}q_0(x, y), \qquad \tau_{xz}(x, y) = 0 \qquad \text{and} \quad \tau_{yz}(x, y) = 0$$

b. at the bottom surface ($z = \frac{h_f}{2}$),

$$\sigma_z(x,y) = \sum_{i=1}^{n_w} {}_i^t Q_{\text{int}}, \qquad \tau_{xz}(x,y) = \sum_{i=1}^{n_w} {}_i^t S_{\text{int}} \qquad \textit{and} \quad \tau_{yz}(x,y) = \sum_{i=1}^{n_w} {}_i^t V_{\text{int}} \tag{24}$$

and for the bottom face-plate are:

a. at the top surface ($z = -\frac{h_f}{2}$),

$$\sigma_z(x,y) = \sum_{i=1}^{n_w} {}_i^b Q_{\text{int}}, \qquad \tau_{xz}(x,y) = \sum_{i=1}^{n_w} {}_i^b S_{\text{int}} \qquad \textit{and} \quad \tau_{yz}(x,y) = \sum_{i=1}^{n_w} {}_i^b V_{\text{int}}$$

b. at the bottom surface ($z = \frac{h_f}{2}$),

$$\sigma_z(x,y) = {}^b q_0(x,y), \qquad \tau_{xz}(x,y) = 0 \qquad \text{and} \quad \tau_{yz}(x,y) = 0 \tag{25}$$

where ${}^t\mathrm{q}_0$ and ${}^b\mathrm{q}_0$ are the applied transverse loads on the top and bottom face-plates respectively, which are taken to be positive when applied downward in the positive z direction. The above equations yield the six unknown constants of the top and bottom face-plates in terms of ${}_i^p Q_m^S$, ${}_i^p Q_m^A$, ${}_i^p S_m^S$, ${}_i^p S_m^A$, ${}_i^p V_m^S$ and the applied transverse loads.

Analysis of the overall structure

With the continuity of interface tractions already satisfied as explained above, the only step left is to enforce the displacement continuity along the interface patch at the top and bottom of each web. Consistent with the approximate models employed for the webs, the following interface continuity conditions are appropriate:

1. Continuity of the u, v and w displacements along the centre line of each interface patch of width B.
2. Continuity of the rotations $w_{,y}$ of the face-plate and $-v_{,z}$ of the web along the centre line of each interface patch of width B (see Figure 3).
3. Continuity of the inplane rotation $u_{,y}$ of a small linear element oriented along the y-direction in the plane of the interface patch for both the face-plate and the web; the small element is located at the centre of the patch (see Figure 3).

The continuity conditions 2 and 3 are necessary in order to maintain the integral nature of the web-core sandwich structure. It is convenient to enforce condition 3

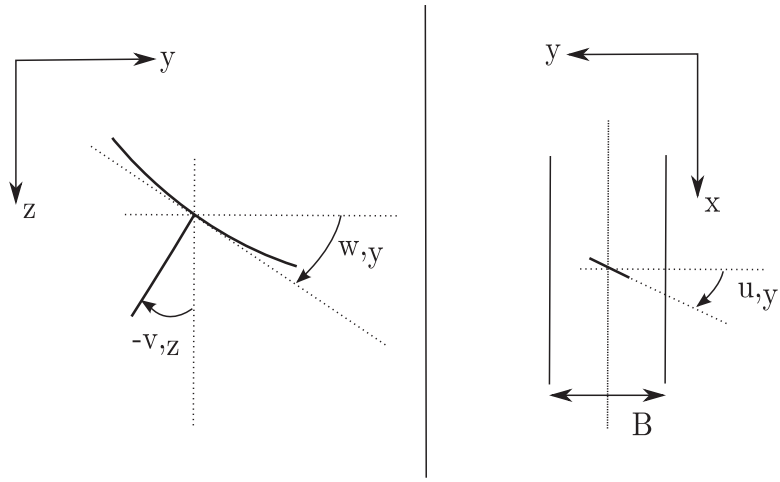

Figure 3. Displacement continuity at the interface.

by ensuring continuity of the shear strain γ_{xy} of the face-plate and the web along the centre line of the interface patch; this is because $\gamma_{xy} = u_{,y} + v_{,x}$ and continuity of $v_{,x}$ is already enforced by virtue of condition 1. The limitation of enforcing the continuity conditions only along the centre line of the interface patch is shown later to be quite satisfactory and one that yields good agreement with the results of full 3-D modelling of both the face-plates and the webs.

Imposing the above continuity conditions and comparing the corresponding Fourier terms results in a set of linear equations in ${}^{p}_{i}Q^{S}_{m}$, ${}^{p}_{i}Q^{A}_{m}$, ${}^{p}_{i}S^{S}_{m}$, ${}^{p}_{i}S^{A}_{m}$ and ${}^{p}_{i}V^{S}_{m}$.

A simpler model based on classical assumptions

In order to study the importance of capturing non-classical effects like transverse shear deformation and thickness stretch in the face-plates, the above rigorous model needs to be compared with one based on the kinematic assumptions of the classical plate theory, namely the hairbrush hypothesis for the face-plates; while doing so, it is important to shift the interface tractions to the mid-plane of the face-plates, as explained below. It should be noted that the webs continue to be analysed as explained earlier, because the transverse shear deformation of the core should always be accounted for in sandwich plate analysis.

Shifting the interface tractions to the mid-plane of the plate results in two additional distributed moments ${}^{p}_{i}m_{px}(x,y)$ and ${}^{p}_{i}m_{py}(x,y)$ per unit area, acting over the interface area a x B between the i^{th} web and the face-plate, besides ${}^{p}_{i}Q_{\text{int}}(x,y)$, ${}^{p}_{i}S_{\text{int}}(x,y)$ and ${}^{p}_{i}V_{\text{int}}(x,y)$ (see equations (21), (22) and (23)). These are given by

$$ {}^{p}_{i}m_{px}(x,y) = \frac{h_f}{2}\cdot{}^{p}_{i}S_{\text{int}}(x,y) = \frac{h_f}{2}\sum_{m=1}^{\infty}\sum_{n=1}^{\infty}\left({}^{p}_{i}S_{mn}\cos\left(\frac{m\pi}{a}x\right)\sin\left(\frac{n\pi}{b}y\right)\right) $$

$$ {}^{p}_{i}m_{py}(x,y) = \frac{h_f}{2}.{}^{p}_{i}V_{\text{int}}(x,y) = \frac{h_f}{2}\sum_{m=1}^{\infty}\sum_{n=1}^{\infty}\left({}^{p}_{i}V_{mn}\sin\left(\frac{m\pi}{a}x\right)\cos\left(\frac{n\pi}{b}y\right)\right) $$

A displacement field given by

$$ w(x,y,z) = w(x,y) $$

$$ u(x,y,z) = u_0(x,y) - z.w_{,x} $$

$$ v(x,y,z) = v_0(x,y) - z.w_{,y} $$

where u_0, v_0 and w are mid-plane displacements, is sufficient to capture the effect of the loading system.

The corresponding equations of equilibrium for the top face-plate are

$$ N_{x,x} + N_{xy,y} + \sum_{i=1}^{n_w} {}^{t}_{i}S_{\text{int}} = 0 \tag{26} $$

$$ N_{xy,x} + N_{y,y} + \sum_{i=1}^{n_w} {}^{t}_{i}V_{\text{int}} = 0 \tag{27} $$

$$ M_{x,x} + M_{xy,y} + \sum_{i=1}^{n_w} {}^{t}_{i}m_{px} = Q_x \tag{28} $$

$$ M_{xy,x} + M_{y,y} + \sum_{i=1}^{n_w} {}^{t}_{i}m_{py} = Q_y \tag{29} $$

$$ Q_{x,x} + Q_{y,y} + \sum_{i=1}^{n_w} {}^{t}_{i}Q_{\text{int}} + {}^{t}\,q_0 = 0 \tag{30} $$

wherein N_j, M_j and Q_j are the usual stress resultants of plate theory and ${}^{t}\mathrm{q}_0$ is the transverse load applied on the top face-plate.

Eliminating Q_x and Q_y from (30) using (28) and (29), we have

$$ M_{x,xx} + 2M_{xy,xy} + M_{y,yy} + \sum_{i=1}^{n_w}({}^{t}_{i}Q_{\text{int}} + {}^{t}_{i}m_{px,x} + {}^{t}_{i}m_{py,y}) + {}^{t}\,q_0 = 0 \tag{31} $$

Using the plane stress-reduced constitutive law for the plate as given by

$$ \begin{Bmatrix} \sigma_x \\ \sigma_y \\ \tau_{xy} \end{Bmatrix} = \begin{bmatrix} Q_{11} & Q_{12} & 0 \\ Q_{12} & Q_{22} & 0 \\ 0 & 0 & Q_{66} \end{bmatrix} \begin{Bmatrix} \epsilon_x \\ \epsilon_y \\ \gamma_{xy} \end{Bmatrix} $$

and obtaining the generalized force displacement relations by appropriate integration over the thickness of the plate, the governing equations of the top face-plate can be derived as

$$A_{11}u_{0,xx} + A_{12}v_{0,xy} + A_{66}(u_{0,yy} + v_{0,xy}) = -\sum_{i=1}^{n_w} {}^{t}_{i}S_{\text{int}}$$

$$A_{66}(u_{0,xy} + v_{0,xx}) + A_{12}u_{0,xy} + A_{22}v_{0,yy} = -\sum_{i=1}^{n_w} {}^{t}_{i}V_{\text{int}}$$

$$D_{11}w_{,xxxx} + D_{22}w_{,yyyy} + (2D_{12} + 4D_{66})w_{,xxyy} = \sum_{i=1}^{n_w}({}^{t}_{i}Q_{\text{int}} + {}^{t}_{i}m_{px,x} + {}^{t}_{i}m_{py,y}) + {}^{t}q_0$$

where A_{ij} and D_{ij} are defined as

$$(A_{ij}, D_{ij}) = \int_{-h/2}^{h/2} Q_{ij}(1, z^2)\mathrm{d}z$$

Similarly, the governing equations of the bottom face-plate are derived as

$$A_{11}u_{0,xx} + A_{12}v_{0,xy} + A_{66}(u_{0,yy} + v_{0,xy}) = \sum_{i=1}^{n_w} {}^{b}_{i}S_{\text{int}}$$

$$A_{66}(u_{0,xy} + v_{0,xx}) + A_{12}u_{0,xy} + A_{22}v_{0,yy} = \sum_{i=1}^{n_w} {}^{b}_{i}V_{\text{int}}$$

$$D_{11}w_{,xxxx} + D_{22}w_{,yyyy} + (2D_{12} + 4D_{66})w_{,xxyy} = \sum_{i=1}^{n_w}(-{}^{b}_{i}Q_{\text{int}} + {}^{b}_{i}m_{px,x} + {}^{b}_{i}m_{py,y}) + {}^{b}q_0$$

where ${}^{b}q_0$ is the transverse load applied on the bottom face-plate. In the above equations, A_{ij} and D_{ij} correspond to the stiffness coefficients Q_{ij} of the bottom face-plate.

A solution of the form

$$w(x, y) = \sum_{m=1}^{\infty}\sum_{n=1}^{\infty} W_{mn}\sin\left(\frac{m\pi}{a}x\right)\sin\left(\frac{n\pi}{b}y\right)$$

$$u_0(x, y) = \sum_{m=1}^{\infty}\sum_{n=1}^{\infty} U_{mn}\cos\left(\frac{m\pi}{a}x\right)\sin\left(\frac{n\pi}{b}y\right)$$

$$v_0(x,y) = \sum_{m=1}^{\infty}\sum_{n=1}^{\infty} V_{mn} \sin\left(\frac{m\pi}{a}x\right)\cos\left(\frac{n\pi}{b}y\right)$$

ensures that the shear-diaphragm type simple support conditions for both the face-plates:

$$\text{at } x = 0,\ a; \quad w = 0, \quad M_x = 0, \quad N_x = 0, \quad v = 0$$

$$\text{at } y = 0,\ b; \quad w = 0, \quad M_y = 0, \quad N_y = 0, \quad u = 0$$

are satisfied a priori.

Substitution of the displacements in the governing equations yields U_{mn}, V_{mn} and W_{mn} in terms of ${}^{p}_{i}Q^{S}_{m}$, ${}^{p}_{i}Q^{A}_{m}$, ${}^{p}_{i}S^{S}_{m}$, ${}^{p}_{i}S^{A}_{m}$, ${}^{p}_{i}V^{S}_{m}$ and the applied transverse loads for each face-plate.

Subsequent steps involving enforcement of displacement continuity along the web-face-plate interfaces to determine the unknown traction coefficients are similar to the ones explained earlier in section 2.4.

Results and discussion

Before proceeding with numerical studies, the acceptability of the assumptions made in the above analytical formulation (denoted by 3D-PS, 3D elasticity for the face-plates and plane stress for the webs) is verified by comparison with a full three-dimensional finite element study (denoted by 3D-3D). The face-plates and the webs are discretized using 20-noded Solid 186 elements in ANSYS. A mesh involving four elements across the web depth, two elements across the web breadth and two elements across the face-plate thickness is found to yield convergent results. The problems considered are simply supported square web-core sandwich plates with five equally spaced webs, subjected to a uniform downward load distributed equally on the top and bottom face-plates. Two materials are considered – one isotropic with $\nu = 0.3$, and the other a unidirectional fibre composite with the fibres and webs running along the x direction and with properties given by $E_L/E_T = 25$, $G_{LT}/E_T = 0.5$, $G_{TT}/E_T = 0.2$ and $\nu_{LT} = \nu_{TT} = 0.25$, typical of graphite-epoxy.

The central deflections and critical inplane stresses (σ_x and σ_y) of the top face-plate are shown in Tables 1 and 2. Figure 4 shows the variation of the non-dimensionalized deflections and inplane stresses along the span of the top face-plate. For all cases, the breadth B of the webs are taken to be equal to the thickness h_f of the face-plate. The number of terms taken (m_{max}, n_{max}) in the Fourier series used in the present formulation is of the order of (40, 400) to obtain good convergence of the final results.

As can be seen from Tables 1 and 2, the deflections and stresses are predicted quite accurately even for deep webs ($a/H = 15$). The 3D-PS model is also able to

Table 1. Isotropic web-core sandwich plate with five webs.

		$\frac{w_{centre}E}{q_0}\frac{h_f^3}{a^4}\times 10^5$			$\frac{10\sigma_x(a/2,a/2,-h_f/2)}{q_0(\frac{a}{h_f})^2}$			$\frac{10\sigma_y(a/2,a/6,-h_f/2)}{q_0(\frac{a}{h_f})^2}$		
a/h_f	H/h_f	3D-PS	3D-3D	% Error[a]	3D-PS	3D-3D	% Error	3D-PS	3D-3D	% Error
60	4	88.47	90.34	−2.1	−0.221	−0.226	−2.2	−0.320	−0.305	4.9
120	4	82.39	83.26	−1.0	−0.219	−0.222	−1.4	−0.301	−0.291	3.4

[a]Error of 3D-PS with respect to 3D-3D.

Table 2. Orthotropic web-core sandwich plate with five webs.

		$\frac{w_{centre}E_T}{q_0}\frac{h_f^3}{a^4}\times 10^5$			$\frac{10\sigma_x(a/2,a/2,-h_f/2)}{q_0(\frac{a}{h_f})^2}$			$\frac{10\sigma_y(a/2,a/10,-h_f/2)}{q_0(\frac{a}{h_f})^2}$		
a/h_f	H/h_f	3D-PS	3D-3D	% Error	3D-PS	3D-3D	% Error	3D-PS	3D-3D	% Error
60	4	18.73	18.28	2.4	−0.543	−0.540	0.6	−0.093	−0.090	3.3
120	4	13.25	13.01	1.8	−0.530	−0.529	0.1	−0.081	−0.080	∼0

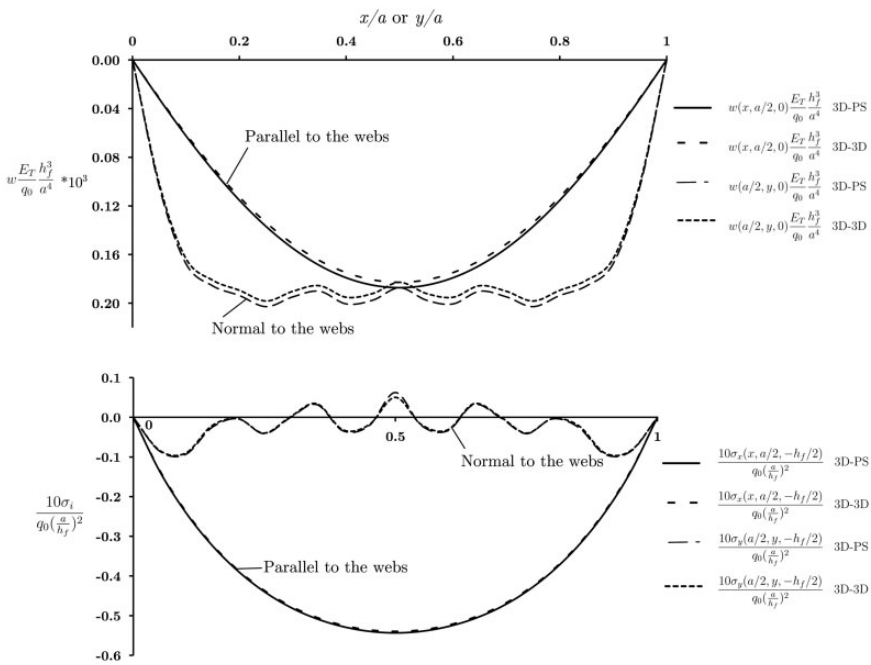

Figure 4. Displacement and stress fields for an orthotropic web-core sandwich plate with $a/h_f = 60$, $H/h_f = 4$, $B/h_f = 1$ and $n_w = 5$.

precisely capture the secondary bending of the face-plates between the webs, which manifests as sudden changes in curvatures of the deflection field perpendicular to the directions of the webs and waviness in the σ_y stress field (Figure 4). This indicates that the plane stress idealization employed for the webs in the transverse x–z plane and the simple one-dimensional lateral bending and torsion models are quite adequate to model the kinematics of the webs and that enforcement of the associated interface continuity conditions only along the centre line of each interface patch is sufficient. Further, the assumed constant and linear components of the interface tractions (see Figure 2) are also proved to be adequate.

Static flexure results derived from the present formulation are now generated for simply supported isotropic and orthotropic square web-core plates of various thicknesses. These are compared to results based on the classical approach denoted by CPT-PS (i.e. Classical Plate Theory for the face-plates and plane stress for the webs). The central deflections and critical inplane stresses (σ_x and σ_y) at the top face-plate are tabulated while non-dimensionalized deflections and inplane stress fields are plotted along the span of the top face-plate. The following cases are considered:

1. Bare isotropic and orthotropic square plates (Table 3).
2. Isotropic web-core sandwich plates with five (Table 4 and Figure 5) and seven (Table 5 and Figure 6) equally spaced webs.
3. Orthotropic web-core sandwich plates with five (Table 6 and Figure 7) and seven (Table 7 and Figure 8) equally spaced webs oriented parallel to the fibers.

The material properties are taken as for Tables 1 and 2. Further, the breadth B of each web is taken to be equal to the thickness h_f of the face-plates.

From these results, the following observations may be noted:

1. For all cases, the CPT-PS results of deflections are under-predictions as expected.

Table 3. Bare plate.

	Isotropic Plate			Orthotropic Plate		
	$\frac{w_{centre}E}{q_0}\frac{h^3}{a^4} \times 10^3$			$\frac{w_{centre}E_T}{q_0}\frac{h^3}{a^4} \times 10^4$		
a/h	CPT	3D	% Error[a]	CPT	3D	% Error[a]
60	44.36	44.42	−0.1	64.97	65.82	−1.3
80	44.36	44.39	−0.1	64.97	65.45	−0.7
120	44.36	44.38	0.0	64.97	65.18	−0.3

[a]Error of CPT with respect to 3D elasticity.

Table 4. Isotropic web-core sandwich plate with five webs.

		$\frac{w_{centre}E}{q_0}\frac{h_f^3}{a^4}\times 10^5$			$\frac{10\sigma_x(a/2,a/2,-h_f/2)}{q_0(\frac{a}{h_f})^2}$			$\frac{10\sigma_y(a/2,a/6,-h_f/2)}{q_0(\frac{a}{h_f})^2}$		
a/h_f	H/h_f	CPT-PS	3D-PS	% Error[a]	CPT-PS	3D-PS	% Error	CPT-PS	3D-PS	% Error
60	4	80.76	88.47	−8.7	−0.208	−0.221	−5.8	−0.350	−0.320	9.3
80	2	157.7	166.1	−5.0	−0.315	−0.325	−3.0	−0.612	−0.602	1.6
120	4	78.18	82.39	−5.1	−0.212	−0.219	−3.2	−0.324	−0.301	7.6

[a]Error of CPT-PS with respect to 3D-PS.

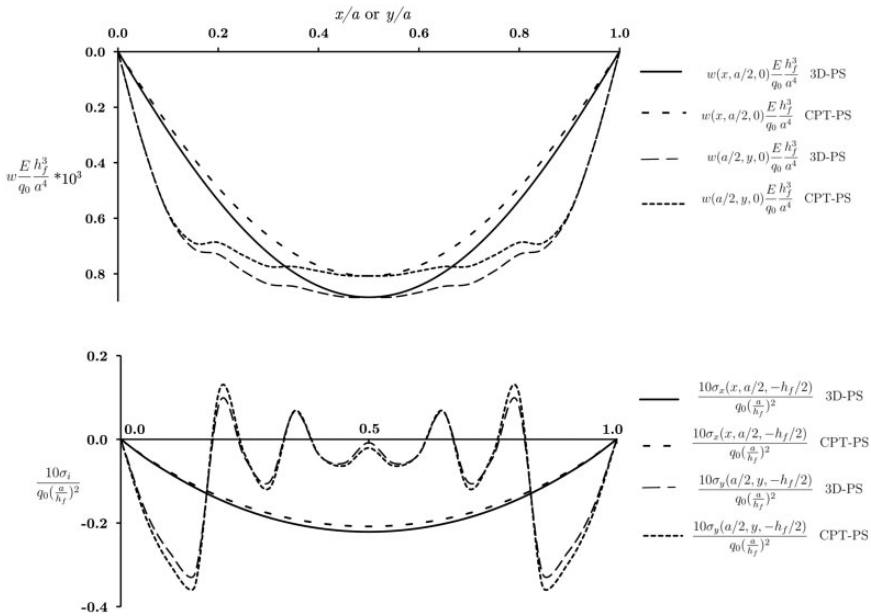

Figure 5. Displacement and stress fields for an isotropic web-core sandwich plate with $a/h_f=60$, $H/h_f=4$, $B/h_f=1$ and $n_w=5$.

Table 5. Isotropic web-core sandwich plate with seven webs.

		$\frac{w_{centre}E}{q_0}\frac{h_f^3}{a^4}\times 10^5$			$\frac{10\sigma_x(a/2,a/2,-h_f/2)}{q_0(\frac{a}{h_f})^2}$			$\frac{10\sigma_y(a/2,a/10,-h_f/2)}{q_0(\frac{a}{h_f})^2}$		
a/h_f	H/h_f	CPT-PS	3D-PS	% Error	CPT-PS	3D-PS	% Error	CPT-PS	3D-PS	% Error
60	4	62.71	71.55	−12.4	−0.175	−0.193	−9.3	−0.403	−0.356	13.1
80	2	124.8	132.3	−5.7	−0.268	−0.277	−3.2	−0.578	−0.565	2.3
120	4	61.79	66.74	−7.4	−0.180	−0.191	−5.7	−0.381	−0.353	7.9

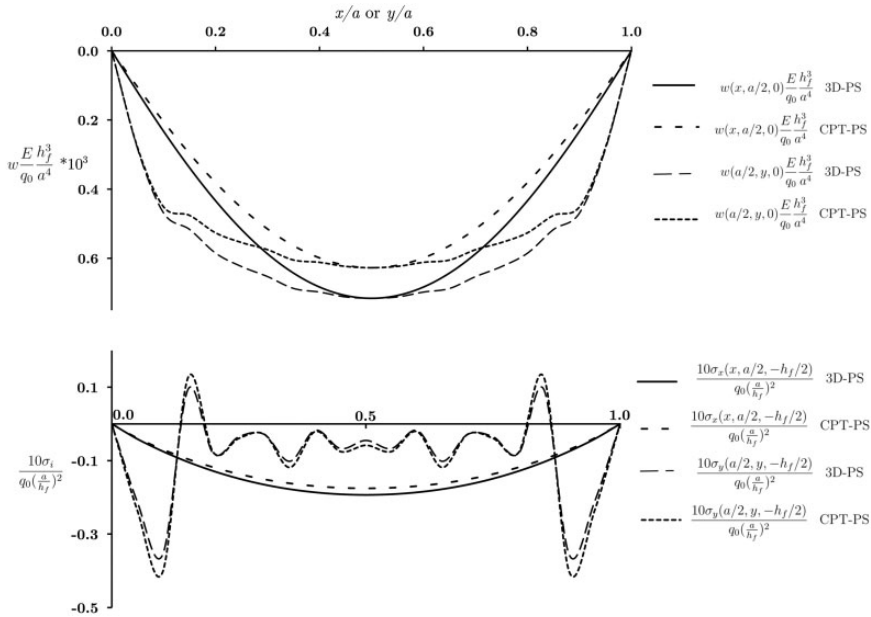

Figure 6. Displacement and stress fields for an isotropic web-core sandwich plate with $a/h_f = 60$, $H/h_f = 4$, $B/h_f = 1$ and $n_w = 7$.

Table 6. Orthotropic web-core sandwich plate with five webs.

		$\frac{w_{centre}E_T}{q_0}\frac{h_f^3}{a^4}\times 10^5$			$\frac{10\sigma_x(a/2,a/2,-h_f/2)}{q_0(\frac{a}{h_f})^2}$			$\frac{10\sigma_y(a/2,a/10,-h_f/2)}{q_0(\frac{a}{h_f})^2}$		
a/h_f	H/h_f	CPT-PS	3D-PS	% Error	CPT-PS	3D-PS	% Error	CPT-PS	3D-PS	% Error
60	4	17.31	18.73	−7.6	−0.565	−0.543	4.1	−0.095	−0.093	2.1
80	2	29.17	32.01	−8.9	−0.972	−0.957	1.5	−0.123	−0.124	−1.0
120	4	12.53	13.25	−5.4	−0.541	−0.530	2.0	−0.081	−0.081	0

2. The central deflection error of CPT-PS with respect to 3D-PS (fifth column in Tables 4 to 7) is a combination of the effects of non-classical phenomena, namely transverse shear deformation and thickness stretch. It has been shown (see, for example, [20]) that the effect of shear deformation is always more significant than thickness stretch, so this error will be referred to hereafter as the shear deformation effect. This error is clearly significant (around 7%) even in web-core sandwich plates with thin face-plates ($a/h_f = 120$) and seems equally pronounced in isotropic as well as orthotropic web-core plates. This has to be contrasted with the results of the bare plate with the same a/h in Table 3 where

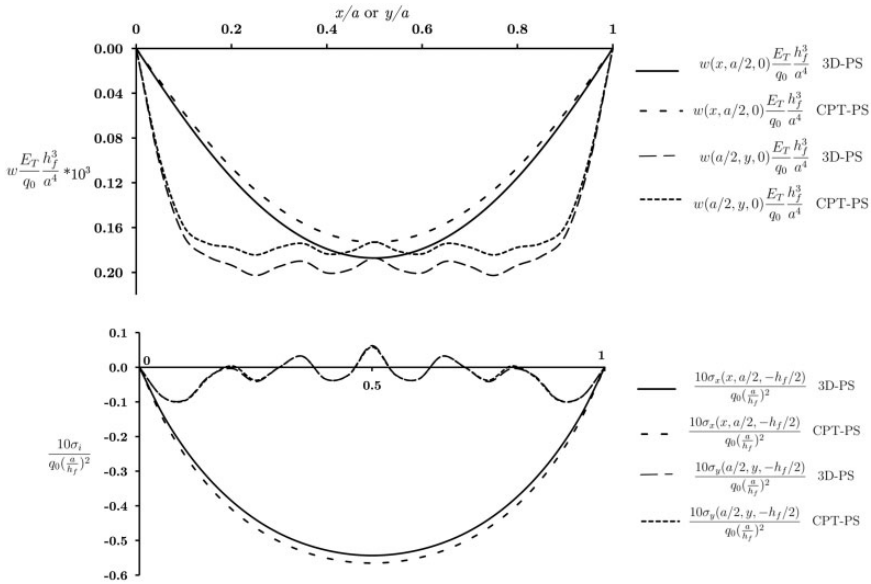

Figure 7. Displacement and stress fields for an orthotropic web-core sandwich plate with $a/h_f = 60$, $H/h_f = 4$, $B/h_f = 1$ and $n_w = 5$.

Table 7. Orthotropic web-core sandwich plate with seven webs.

		$\frac{w_{centre}E_T}{q_0}\frac{h_f^3}{a^4} \times 10^5$			$\frac{10\sigma_x(a/2,a/2,-h_f/2)}{q_0(\frac{a}{h_f})^2}$			$\frac{10\sigma_y(a/2,a/10,-h_f/2)}{q_0(\frac{a}{h_f})^2}$		
a/h_f	H/h_f	CPT-PS	3D-PS	% Error	CPT-PS	3D-PS	% Error	CPT-PS	3D-PS	% Error
60	4	13.49	14.61	−7.6	−0.457	−0.442	3.4	−0.085	−0.074	14.9
80	2	23.51	25.69	−8.5	−0.801	−0.789	1.5	−0.123	−0.121	1.8
120	4	9.87	10.43	−5.3	−0.440	−0.433	1.6	−0.062	−0.058	7.0

the errors are less than 0.3%. Thus, while the plate can be modelled as "thin" when used alone, such an idealization leads to significant errors when the same plate is part of the sandwich construction. This is an important observation that should be kept in mind while developing discrete models for sandwich plates.

3. The deflection plots perpendicular to the direction of the webs in Figures 5 to 8 reveal the prominent secondary bending effects of the face-plates between the webs. This is characterized by abrupt changes in the curvature of the deformations between the webs, with the waviness increasing as the number of webs increases. This effect is more severe in the case of orthotropic web-core sandwich plates because of the low bending stiffness of the plate in the direction perpendicular to the webs. For such cases, it is further observed that the point of

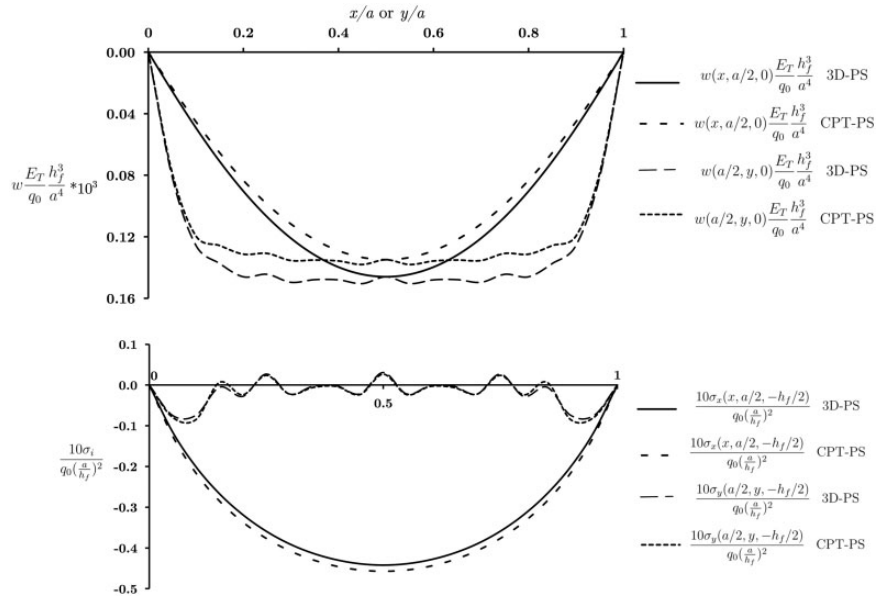

Figure 8. Displacement and stress fields for an orthotropic web-core sandwich plate with $a/h_f = 60$, $H/h_f = 4$, $B/h_f = 1$ and $n_w = 7$.

maximum deflection shifts away from the centre of the plate to a point between the webs. While the CPT-PS model is able to capture the qualitative aspects of the secondary bending of the face-plates, it is evident that accounting for the shear deformation of the face-plates is important to get accurate estimates of deflections at specific points.

4. Critical values of the bending stresses (σ_x and σ_y) as calculated by both models are shown in Tables 4 to 7. For any particular configuration of webs, the errors of the CPT-PS model for the stresses are comparable to those for the deflections. These stress errors are significant even for fairly thin face-plates ($a/h_f = 80$), indicating the importance of using thick face-plate kinematics for accurate stress analysis.
5. The stress fields plotted in Figures 5 to 8 depict the effect of secondary bending of the face-plates on the bending stress σ_y. The sudden changes in curvature of the deformations of the face-plates between the webs cause this stress to oscillate between being tensile and compressive, with the point of maximum σ_y occurring between the webs away from the centre of the plate. For orthotropic web-core plates, this stress is not expected to be very important (because of the low bending stiffness of the face-plate in this direction), but for isotropic web-core plates, this stress is clearly significant and even dominates over σ_x. Again, while the CPT-PS model is able to exhibit the general trends of the stress field well, it is unable to accurately capture the peak values.

Finally, a physical case study is presented to illustrate the difference in the flexural behaviour of a web-core sandwich plate and a homogeneous bare plate; this clearly shows the importance of employing discrete models for the accurate analysis of web-core sandwich plates.

A simply-supported bare aluminium plate ($E = 70\,\text{GPa}$ and $\nu = 0.3$) of dimensions $1000\,\text{mm} \times 1000\,\text{mm} \times 50\,\text{mm}$ is subjected to a uniformly distributed load $q_0 = 100\,\text{kPa}$ on the top surface. The displacements and stress fields are computed using the 3D equations of elasticity. The same load is also applied on the top face-sheet of a web-core sandwich plate of the same total thickness (50 mm) as that of the bare plate. The face-sheets have dimensions of $1000\,\text{mm} \times 1000\,\text{mm} \times 8.4\,\text{mm}$ while the webs have cross-section dimensions $B = 8.4\,\text{mm}$ and $H = 33.3\,\text{mm}$. Three separate cases are considered with three, five and seven equally spaced webs.

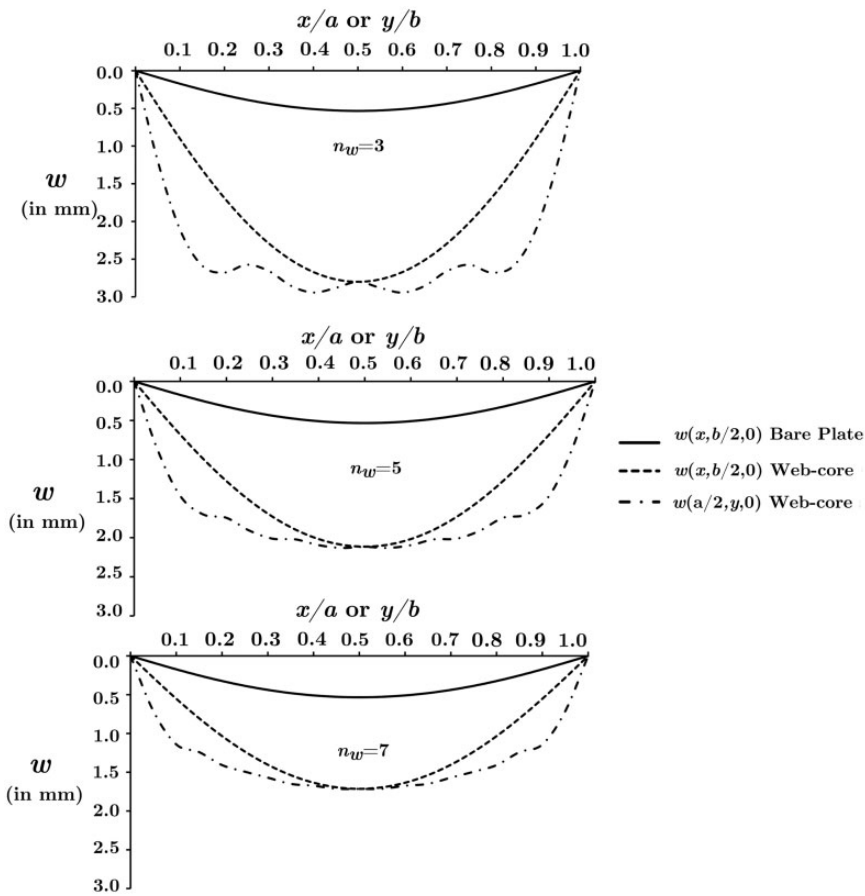

Figure 9. Comparison of displacement fields.

The web-core sandwich plate is made of the same material as the bare plate. Displacement and stress fields as determined by the 3D-PS model are plotted along the midlines of the top-face plates and are compared with those of the bare plate in Figures 9 and 10.

From these plots, it is observed that:

1. Since the total thickness of the homogeneous plate and web-core sandwich plate are the same, the latter represents the case of material being removed from a bare plate. Hence the displacement and bending stresses in the sandwich plate are greater than those of the bare plate and are significantly influenced by secondary bending effects, as explained below.
2. Due to the local secondary bending of the face-plates between the webs, the deformation and stress fields of web-core sandwich plates are characteristically

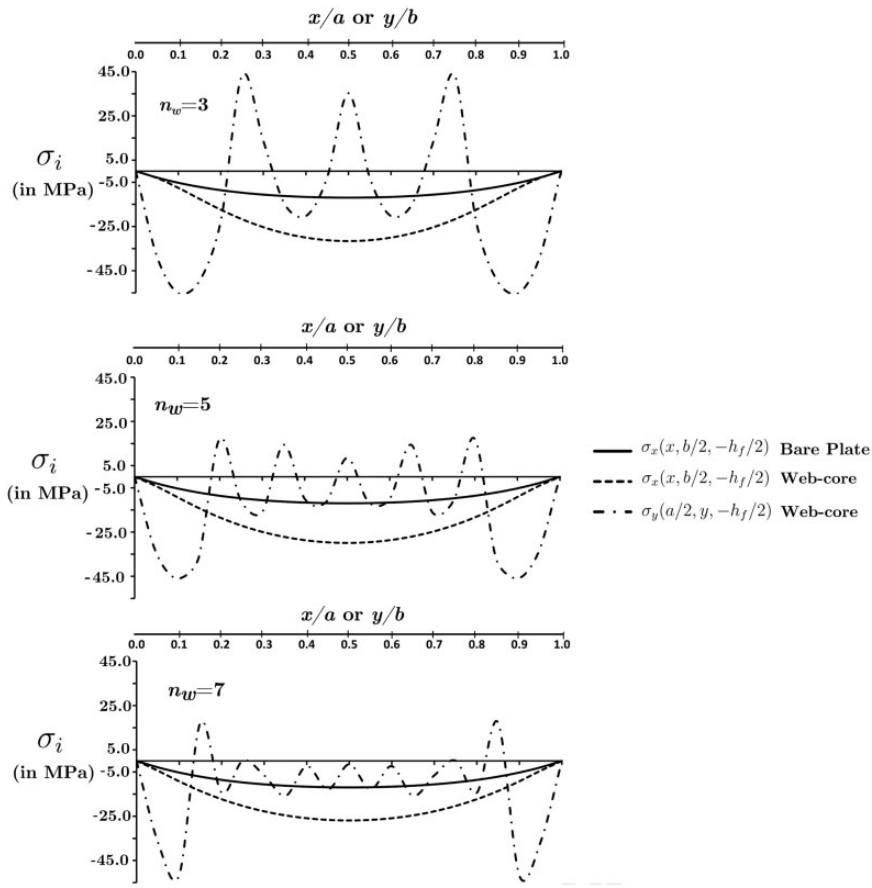

Figure 10. Comparison of stress fields.

different from those of a homogeneous bare plate. Sudden changes of curvatures of the transverse deflections perpendicular to the direction of the webs causes the σ_y bending stress to oscillate between being tensile and compressive in web-core sandwich plates. Further, the point of maximum σ_y shifts away from the centre of the plate to a point between the support and the first web, and is much larger in magnitude than the critical value of σ_x. On the other hand, the deflection and stress fields of the homogenous plate in both the perpendicular directions show no sudden variations, with the points of maximum deflection and stresses lying in the centre of the plate as expected. This clearly indicates the importance of using discrete models to capture the localized secondary bending effects in web-core sandwich plates for accurate displacement and stress analysis.

3. As the number of webs increase, the maximum deflections in the sandwich plate reduce and the effects of secondary bending or "waviness" of the face plates between the webs become more localized. Interestingly, with an increase in the number of webs, the maximum stresses do not reduce significantly despite the decrease in amplitude of the oscillatory σ_y stress.

Conclusion

An accurate discrete model for simply supported web-core plates is presented which completely accounts for the non-classical effects of transverse shear deformation and transverse thickness-stretch in the face-plates and the webs. This model is capable of accurately capturing the secondary local bending effects of the face-plates between the webs on the displacement and stress fields. Further, it is shown that the lateral bending and torsion of the webs can be satisfactorily modelled using classical one-dimensional theories. Results obtained by this rigorous approach are used to highlight the errors of the commonly used model based on the classical hairbrush hypothesis for the face-plates. It has clearly been shown that even a plate that can be modelled using the classical thin-plate theory when used as a bare plate needs to be considered as thick when it is used as a sandwich face-plate.

Declaration of Conflicting Interests

The author(s) declared no potential conflicts of interest with respect to the research, authorship, and/or publication of this article.

Funding

The author(s) received no financial support for the research, authorship, and/or publication of this article.

References

1. Zenkert D. *The handbook of sandwich construction*. Warrington: EMAS Publishing, 1997.
2. Frostig Y, Baruch M, Vilnay O, et al. High-order theory for sandwich-beam behavior with transversely flexible core. *J Eng Mech* 1992; 118(5): 1026–1043.

3. Frostig Y. Elastica of sandwich panels with a transversely flexible core- a high-order theory approach. *Int J Solids Struct* 2009; 46(11): 2043–2059.
4. Meyer-Piening H. Application of the elasticity solution to linear sandwich beam, plate and shell analyses. *J Sandwich Struct Mater* 2004; 6(4): 295–312.
5. Burton W and Noor A. Three-dimensional solutions for thermomechanical stresses in sandwich panels and shells. *J Eng Mech* 1994; 120(10): 2044–2071.
6. Kapania R, Soliman H, Vasudeva S, et al. Static analysis of sandwich panels with square panels with square honeycomb core. *AIAA Journal* 2008; 46(3): 627–634.
7. Nordstrand T, Carlsson L and Allen H. Transverse shear stiffness of structural core sandwich. *Composite Structures* 1994; 27(3): 317–329.
8. Xia Y, Friswell M and Flores E. Equivalent models of corrugated panels. *Int J Solids Struct* 2012; 49(13): 1453–1462.
9. Cheng Q, Lee H and Lu C. A numerical analysis approach for evaluating elastic constants of sandwich structures with various cores. *Composite Structures* 2006; 74(2): 226–236.
10. Lok T and Cheng Q. Elastic deflection of thin-walled sandwich panel. *J Sandwich Struct Mater* 1999; 1(4): 279–298.
11. Fung T, Tan K and Lok T. Elastic constants for z-core sandwich panels. *J Struct Eng* 1994; 120(10): 3046–3055.
12. Bartolozzi G, Baldanzini N and Pierini M. Equivalent properties for corrugated cores of sandwich structures: A general analytical method. *Composite Structures* 2014; 108: 736–746.
13. Burton W and Noor A. Assessment of computational models for sandwich panels and shells. *Comput Meth Appl Mech Eng* 1995; 124(1): 125–151.
14. Burton W and Noor A. Assessment of continuum models for sandwich panel honeycomb cores. *Comput Meth Appl Mech Eng* 1997; 145(3): 341–360.
15. Romanoff J and Varsta P. Bending response of web-core sandwich plates. *Composite Structures* 2007; 81(2): 292–302.
16. Liu J, Cheng Y, Li R, et al. A semi-analytical method for bending, buckling, and free vibration analyses of sandwich panels with square-honeycomb cores. *Int J Struct Stabil Dyn* 2010; 10(1): 127–151.
17. He L, Cheng Y and Liu J. Precise bending stress analysis of corrugated-core, honeycomb-core and x-core sandwich panels. *Composite Structures* 2012; 94(5): 1656–1668.
18. Bhaskar K and Pydah A. An elasticity approach for simply-supported isotropic and orthotropic stiffened plates. *Int J Mech Sci* 2014; 89: 21–30.
19. Pydah A and Bhaskar K. Accurate discrete modelling of stiffened isotropic and orthotropic rectangular plates. *Thin-Walled Structures*, (under review).
20. Bhaskar K and Varadan TK. *Theory of isotropic/orthotropic elasticity*. Boca Raton, FL: CRC Press, 2009.